Journal of Materials Chemistry A

RSC Publishing

COMMUNICATION

High performance anodes with tailored catalytic properties for $La_{5.6}WO_{11.4-\delta}$ based proton conducting fuel cells†

Cite this: *J. Mater. Chem. A*, 2013, **1**, 3004

Received 18th December 2012
Accepted 17th January 2013

DOI: 10.1039/c3ta01554h

www.rsc.org/MaterialsA

M. Balaguer,[a] C. Solís,[a] F. Bozza,[b] N. Bonanos[b] and J. M. Serra*[a]

A new generation of anodes for PC-SOFCs based on catalytically promoted $La_{0.75}Ce_{0.1}Sr_{0.15}CrO_{3-\delta}$ (LSCCe) is presented. LSCCe is selected as the electrode backbone structure, due to its superior total conductivity over that of LSC. The infiltration of catalytically highly active nickel nanoparticles into the sintered LSCCe electrode boosted the surface limiting reactions.

In the last few years, there has been research interest in reducing the operation temperature of solid oxide fuel cells (SOFC), which would permit easier and cheaper cell designs. The use of proton conducting electrolytes (PC-SOFCs) allows lowering the operation temperature, while achieving very high fuel utilization, since water is formed at the air electrode, without diluting the fuel.[1] $La_{6-x}WO_y$ (LWO, $0.4 < x < 0.7$)[2] is a promising proton conductor, with high and predominant proton conductivity, and high stability in wet CO_2, under typical fuel cell operating conditions.[3] Electrodes compatible with the LWO electrolyte are currently being investigated.[4] Concerning the anodes, strong requirements entail high electrical conductivity, sufficient protonic conductivity, fast gas transport/exchange through a porous scaffold and fine-grained homogeneous microstructure, aside from high catalytic activity toward hydrogen oxidation. Several nickel-based cermet combinations (Ni/YSZ, Ni/CGO, Ni/$Ba(Ce_{0.8-x}Zr_x)Y_{0.1}O_{3-\delta}$) and the mixed conductor $Sr_{0.94}Ti_{0.9}Nb_{0.1}O_3$ (STN) have been proposed and investigated as SOFC anode materials.[5] However, these systems react with the LWO electrolyte, the reaction between LWO and NiO being especially dramatic.[6] $La_{0.85}Sr_{0.15}CrO_{3-\delta}$ (LSC) based anodes have been recently tested as compatible and promising anode materials for LWO electrolytes, although their operation is limited by surface reaction processes associated with low frequency impedance.[6] Here, the initial LSC electrode was improved stepwise by tackling the two major rate limiting steps identified, *i.e.* electrode total conductivity and surface processes. Firstly, enhancement of the transport properties of the chromite was attempted by doping at A and B perovskite positions (A = Sm, Ce, and Nd and B = Ni, Y, Al, Fe, Ti, Ga, Mn, Zn) and Ce-doped LSC was selected. Secondly, nickel infiltration into the sintered Ce-doped electrode was considered, in order to promote the surface reactions as Ni is a well-known, highly active H_2 bond breaking catalyst.[7] Further, metallic Ni nanoparticles are compatible with LWO under anode operating conditions.[6]

Fig. 1a presents the XRD analysis of the LSCCe powder and the Ni-infiltrated LSCCe anode after reduction and electrochemical characterization. The powder sintered at 1200 °C still present traces of $SrCrO_4$ and CeO_2, which disappear either at higher temperatures or in reducing atmospheres.[10] In fact, the LSCCe anode after testing only shows diffraction peaks corresponding to the chromite, together with the LWO from the electrolyte, Au from the current collector and the Ni catalyst. The lack of any other diffraction peaks that could be assigned to any reaction product indicates the compatibility of the LSCCe with the LWO electrolyte, even after the Ni infiltration. Furthermore, the material shows good stability under working conditions and in CO_2 atmospheres (see ESI Fig. S1† for additional compatibility and stability measurements).

Fig. 1b plots the total conductivity of LSCCe in wet H_2 and D_2 as a function of temperature. For comparison, LSC in $H_2 + H_2O$ (anode operating conditions) is also depicted. LSCCe exhibits higher total conductivity under reducing atmospheres. At this pO_2 range, the conductivity of chromites presents a predominant p-type electronic character[8] and this fact is confirmed for LSCCe by means of d.c. conductivity analysis as a function of pO_2 (ESI Fig. S2†), where the power dependency ($\sigma \propto pO_2^n$) at 700 °C approaches the expected 1/4 in dry conditions. Moreover, ionic (O^{2-} and H^+) transport represents an important

[a]*Instituto de Tecnología Química (Universidad Politécnica de Valencia - Consejo Superior de Investigaciones Científicas), Avenida de los Naranjos s/n, 46022 Valencia, Spain. E-mail: jmserra@itq.upv.es; Fax: +34 963877809; Tel: +34 9638 79448*

[b]*Department of Energy Conversion and Storage Technical University of Denmark – DTU, P.O. Box 49, 4000 Roskilde, Denmark*

† Electronic supplementary information (ESI) available. See DOI: 10.1039/c3ta01554h

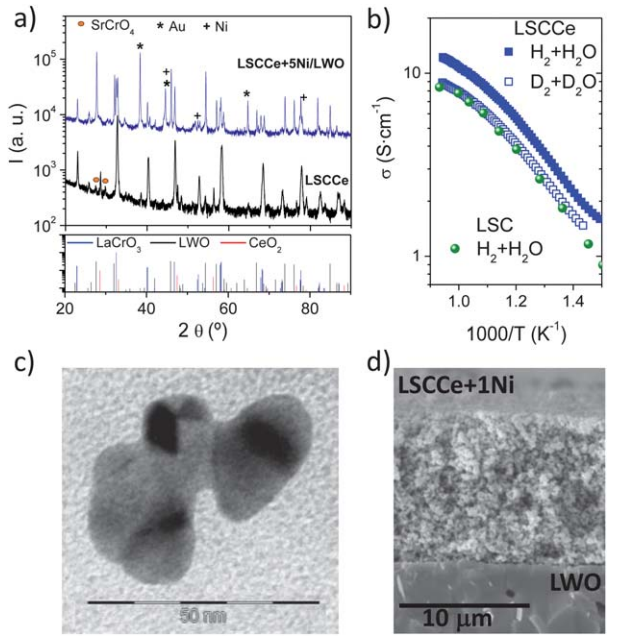

Fig. 1 XRD pattern of the as-prepared LSCCe powder and the LSCCe anode after Ni infiltration and reduction in wet H_2 up to 800 °C (a), LSCCe total conductivity in $H_2 + H_2O$ and $D_2 + D_2O$ and LSC total conductivity in $H_2 + H_2O$ (b), TEM image of Ni nanoparticles obtained by firing nitrate precursor at 800 °C in H_2 (c) and cross-section SEM image of a LSCCe + 1Ni symmetrical cell (d).

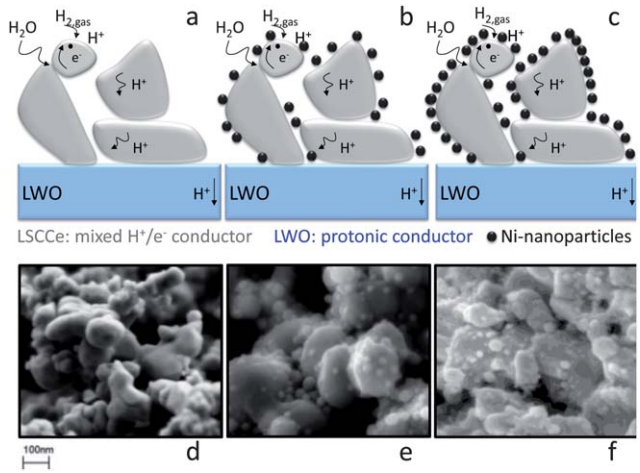

Fig. 2 Schematic diagrams of the LSCCe (a), LSCCe + 1Ni (b) and LSCCe + 5Ni (c) anodes and the corresponding SEM images (d), (e) and (f). 1 M and 5 M water solution of Ni nitrate (LSCe + 1Ni and LSCe + 5Ni, respectively) were dropped on the surface of the electrodes and allowed to penetrate into the electrode pores for 30 min. The infiltration step with the 5 M solution was repeated 4 times. Each infiltration step was followed by calcination at 300 °C to decompose the nitrates.

contribution due to the oxygen vacancies created upon Cr and Ce reduction.[9,10] In wet atmospheres, the isotopic effect (conductivity in $H_2 + H_2O$ is higher than in $D_2 + D_2O$) and the smaller pO_2 dependency (1/6) point out the mixed ionic-protonic transport of the material under these conditions.[6] Due to this mixed electronic-protonic behaviour, one may expect the length of the triple phase boundary (TPB) within the electrode to increase up to the whole electrode surface, enhancing the anode performance.

In order to further improve this anode, different amounts of Ni were incorporated into the sintered anode aiming to study the effect of the catalytic coating on the electrochemical activity. Ni particles of ~10 nm (as observed by TEM in Fig. 1c) resulted from Ni nitrate calcination and subsequent reduction at 800 °C in H_2 (measured in powder). Electrode structural parameters are of great importance especially for infiltrated electrodes, as the pore sizes should host the Ni nanoparticles and allow the mean free path of the gas molecules. The cross-section SEM image of the LSCCe + 1Ni/LWO interface after measurements in reducing conditions (Fig. 1d) shows the highly porous anode layer well-bonded to the electrolyte, which appears to be adequate for proper gas transport. It also shows the very high density of the LWO electrolyte.

The three different LSCCe anodes principally discussed in this work are shown schematically in Fig. 2: (a) LSCCe material, (b) LSCCe infiltrated by using 1 M water solution of Ni nitrate (LSCCe + 1Ni) and (c) LSCCe infiltrated by using 5 M water solution of Ni nitrate (LSCCe + 5Ni). The real SEM images of the cross-section anodes after measurements are shown in Fig. 2d–f, respectively. The study of these three different anodes aims (1) to compare results of the new Ce doped LSC material with previously studied LSC based anodes and (2) to analyse the effect of the surface catalytic promotion due to the Ni infiltration.

SEM images (Fig. 2e and f) provide evidence that the quantity of Ni nanoparticles increases with the Ni concentration of aqueous solution employed in the infiltration. Further, the average Ni particle size is similar (~10 nm) to that shown for the Ni powder reduced from precursor nitrates (Fig. 1c).

Electrochemical properties of the different anodes were analyzed by means of electrochemical impedance spectroscopy (EIS). Spectra at 700 °C in wet H_2 are plotted in ESI Fig. S3a–d.† Polarization resistances (R_p) extracted from EIS at different temperatures (Fig. 3a) for all the studied anodes reflect (1) the improvement reached thanks to the enhancement of transport properties of the backbone chromite material, and (2) the further improvement of the LSCCe anode performance achieved through the infiltration and surface coating with Ni nanoparticles.

The impedance spectra were accurately fitted to a double R//CPE circuit (ESI Fig. S4†) occurring at different characteristic frequencies. Fig. 3b presents the modeled resistances for the pristine LSCCe and the two infiltrated LSCCe electrodes (LSCCe + 1Ni and LSCCe + 5Ni) as a function of temperature (600–800 °C); the corresponding associated capacitances and relaxation times are available in ESI Fig. S5.† The LSCCe anode (Fig. 2a) is principally limited by processes ascribed to low frequencies (LF, 0.3–25 Hz) and this becomes more evident with decreasing temperatures. The LSCCe anode shows another important contribution at medium frequencies (MF, 33–200 Hz). Due to the characteristic frequencies and associated capacitances, both contributions can be related to surface processes, with the MF one being typically associated with surface exchange coupled with bulk ionic transport in mixed conducting electrodes.[11]

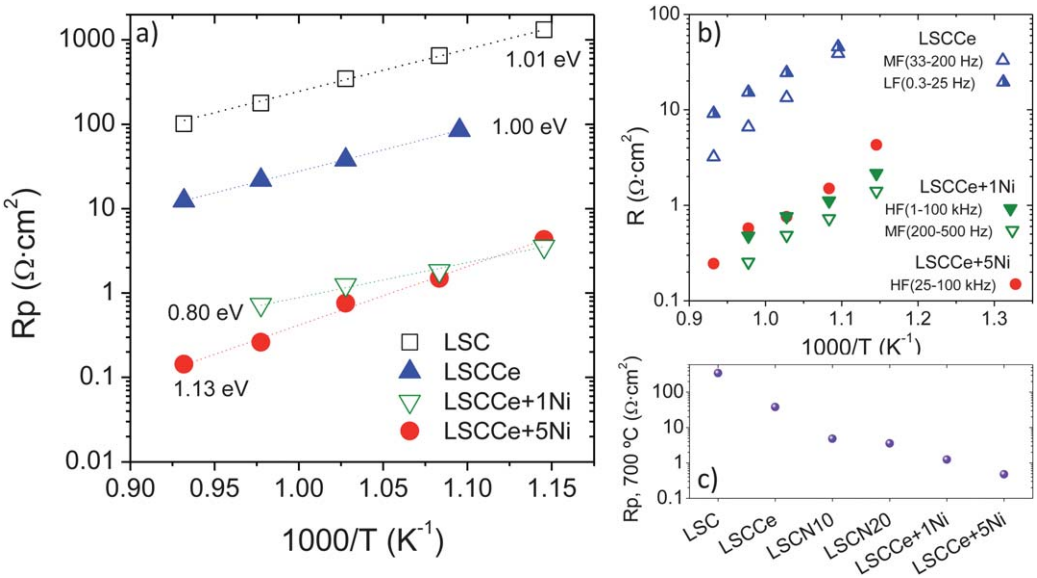

Fig. 3 R_p as a function of the inverse temperature of the four anodes (a), modelled R contributions of the LSCCe anode and when infiltrated with different amounts of Ni (b), and R_p at 700 °C of different chromite anodes ($La_{0.85}Sr_{0.15}CrO_{3-\delta}$ (LSC), $La_{0.75}Ce_{0.1}Sr_{0.15}CrO_{3-\delta}$ (LSCCe), $La_{0.85}Sr_{0.15}Cr_{0.9}Ni_{0.1}O_{3-\delta}$ (LSCN10), $La_{0.85}Sr_{0.15}Cr_{0.8}Ni_{0.2}O_{3-\delta}$ (LSCN20) and LSCCe infiltrated with 1Ni (LSCCe + 1Ni) and with 5Ni (LSCCe + 5Ni)) (c).

With the introduction of a limited amount of Ni nanoparticles (LSCCe + 1Ni, Fig. 2b and e) the LF contribution disappears, the MF associated processes shift to higher frequencies (MF, 200–500 Hz) and a new contribution becomes visible at high frequencies (HF, 1–100 kHz). This confirms the catalytic role of Ni particles, which reduce the surface associated resistances and evidence the surface nature of the abovementioned LF and MF processes. Additionally, the decrease of the LF and MF resistances allows the observation of other, less resistive processes, at higher frequencies. In summary, the reduction of the LF process can be directly linked with the improvement in surface kinetics due to the Ni dispersion on the LSCCe grains.

When the amount of infiltrated Ni is increased (LSCCe + 5Ni, Fig. 2c and f), the MF contribution disappears and only the HF contribution (HF, 25–100 kHz) remains. The HF contribution is ascribed to the transport properties of the LSCCe material or to the LSCCe/LWO interfacial resistances, which remain unchanged upon Ni infiltration. Fig. 3c summarizes the gradual improvement of the anode performance (R_p at 700 °C) throughout the introduction of different changes in the electrode. This figure incorporates the results of LSC electrodes doped with 10 and 20% Ni (partial substitution of Cr in the perovskite), named as LSCN10 and LSCN20, respectively. The reduction of these materials results in the precipitation of catalytic Ni nanoparticles on the LSC grains.[10] This strategy led to the achievement of a R_p value lower than that for the Ce-doped LSC. However, R_p is still better (around one order of magnitude) for the Ni infiltrated LSCCe anodes that present enough catalytic and well-dispersed Ni to strongly boost surface related processes.

Conclusions

This work shows how highly active anode materials for LWO-based proton conducting fuel cells can be engineered by taking into account the operation limitations of the compatible LSC material. Firstly, the synthesis of 10% Ce doped LSC material, its compatibility with LWO and its improved conduction properties are presented. These properties make this composition suitable as an anode material, although EIS analysis revealed that its operation is still limited by LF associated processes related to surface reactions. In order to improve the surface catalytic properties of the anode, Ni infiltration was conducted on the sintered anode, resulting in the coating of the electrode surface with Ni nanoparticles and consequently in a strong improvement of the anode performance. Specifically, the infiltrated anode with the highest Ni loading presents uniquely HF associated resistance and the R_p is 0.26 Ω cm^2 at 750 °C in wet H_2.

Notes and references

1 (*a*) H. Iwahara, *Solid State Ionics*, 1995, **77**, 289; (*b*) E. Fabbri, L. Bi, D. Pergolesi and E. Traversa, *Energy Environ. Sci.*, 2011, **4**, 4984.

2 A more comprehensive formula for LWO is $La_{28-x}W_{4+x}O_{54+3x/2-\delta}$ as reported in ref. 3d, which suggests that the number of oxygen vacancies decreases with x. δ is the oxygen non-stoichiometry related to changes in the oxidation states of the cations.

3 (*a*) R. Haugsrud, *Solid State Ionics*, 2007, **178**, 555; (*b*) R. Haugsrud and C. Kjølseth, *J. Phys. Chem. Solids*, 2008, **69**, 1758; (*c*) C. Solís, S. Escolastico, R. Haugsrud and J. M. Serra, *J. Phys. Chem. C*, 2011, **115**, 11124; (*d*) A. Magraso, J. M. Polfus, C. Frontera, J. Canales-Vazquez, L. Kalland, C. H. Hervoches, S. Erdal, R. Hancke, S. S. Islam, T. Norby and R. Haugsrud, *J. Mater. Chem.*, 2012, **22**, 1762; (*e*) J. M. Serra, S. Escolástico, M. Ivanova, W. Meulenberg, J. Seeger and C. Solís, *Hydrogen permeation through $La_{5.5}WO_{12}$ membranes presented at 10th CMCee – international symposium on ceramic materials and*

components for energy and environmental applications, Dresden, Germany, 20–23 May, 2012.
4 (*a*) C. Solís, L. Navarrete, S. Roitsch and J. M. Serra, *J. Mater. Chem.*, 2012, **22**, 16051; (*b*) E. Quarez, K. V. Kravchyk and O. Joubert, *Solid State Ionics*, 2012, **216**, 19.
5 (*a*) F. Meschke, F. J. Dias and F. Tietz, *J. Mater. Sci.*, 2001, **36**, 5719; (*b*) A. M. Hussain, J. V. T. Høgh, T. Jacobsen and N. Bonanos, *Int. J. Hydrogen Energy*, 2012, **37**, 4309; (*c*) J. M. Serra and W. A. Meulenberg, *J. Am. Ceram. Soc.*, 2007, **90**, 2082; (*d*) S. Ricote and N. Bonanos, *Solid State Ionics*, 2010, **181**, 694.
6 C. Solís, V. B. Vert, M. Balaguer, S. Escolástico, S. Roitsch and J. M. Serra, *ChemSusChem*, 2012, **5**, 2155.
7 (*a*) J. Sfeir, *J. Power Sources*, 2003, **118**, 276; (*b*) T. Caillot, G. Gauthier, P. Delichère, C. Cayron and F. J. Cadete Santos Aires, *J. Catal.*, 2012, **290**, 158; (*c*) A. Atkinsion, S. Barnett, R. J. Gorte, J. T. S. Irvine, A. J. McEvoy, M. Mogensen, S. X. Singhai and J. Vohs, *Nat. Mater.*, 2004, **3**, 14.
8 (*a*) A. L. Sauvet and J. T. S. Irvine, *Solid State Ionics*, 2004, **167**, 1; (*b*) W. Z. Zhu and S. C. Deevi, *Mater. Sci. Eng., A*, 2003, **348**, 227.
9 C. Solís and J. M. Serra, *Solid State Ionics*, 2011, **190**, 38.
10 (*a*) V. B. Vert, F. V. Melo, L. Navarrete and J. M. Serra, *Appl. Catal., B*, 2012, **346**, 115; (*b*) X. Dong, S. Ma, K. Huang and F. Chen, *Int. J. Hydrogen Energy*, 2012, **37**, 10866.
11 (*a*) E. Barsoukov and J. R. Macdonald, *Impedance Spectroscopy Theory, Experiment, and Applications*, John Wiley & Sons, Inc, 2005; (*b*) S. B. Adler, J. A. Lane and B. C. H. Steele, *J. Electrochem. Soc.*, 1996, **143**, 3554.